(Received 5 June 2024, Accepted 22 July 2024, Scheduled 9 August 2024)

High-Isolation Compact MIMO Antenna with Distributed Metamaterial Loading

Zhi Song[1], Shucheng Zhao[1], Siqi Li[1], Jiayi Chen[2], and Yanbing Xue[2,*]

[1] The School of Computer and Communication Engineering, Dalian Jiaotong University, China
[2] The School of Automation and Electrical Engineering, Dalian Jiaotong University, China

ABSTRACT: This paper details the design and realization of a high-isolation multiple-input-multiple-output (MIMO) antenna tailored for fifth-generation (5G) wireless applications. The antenna consists of a 2-element array, with each unit being a patch antenna loaded with six uniformly sized complementary split ring resonators (CSRRs). These CSRRs are strategically etched to minimize the antenna's overall size. In addition, the fragment-type split ring resonators (SRRs) are horizontally positioned between the antenna units to further improve isolation. The placement and structure of these fragment-type SRRs are optimized through a combined use of High-Frequency Structure Simulator (HFSS) and genetic algorithm (GA) techniques, which enables significant isolation levels exceeding −40 dB between antenna units. The proposed MIMO antenna operates within the 5G C-band with a −10 dB bandwidth ranging from 4.84 to 5.00 GHz, while the isolation at 4.9 GHz improves from 14.73 dB to 42.88 dB. Moreover, the maximum Envelope Correlation Coefficient is 0.0042, and the antenna dimensions are 50 mm × 44 mm × 1.6 mm. Antenna samples are fabricated using wet etching on an FR4 substrate. The measured and simulated values are found to be in good agreement. Compared to the traditional antenna design method, which relies on parameters sweeping, the algorithmic approach used in this paper significantly enhances both the design's effectiveness and efficiency.

1. INTRODUCTION

In recent years, the rapid development of wireless communication technology has brought significant attention to the fifth generation (5G) New Radio (NR) and positioned it as one of the most prominently discussed technologies in the field [1]. In addition, multiple-input-multiple-output (MIMO) technology has become one of the core technologies due to its promising features, such as increased data rates and higher capacity. MIMO antennas need to be smaller to meet the miniaturization of 5G communication systems [2]. However, other characteristics of the MIMO antenna are reduced due to the compactness of multiple antennas [3]. Therefore, it is still a main challenge to achieve high isolation between two closely arranged antenna elements in 5G MIMO antenna design [4].

Different approaches to improve the high isolation among closely space antennas have been reported in the literature such as neutralization lines [5], defected ground structures (DGS) [6], electromagnetic bandgap structures (EBG) [7], slits and slots etching approaches [8], antennas orthogonally polarized technique [9–11], irregular parasitic elements [12], and metamaterial (MTM) structures [13]. Among these approaches, enhancing the isolation of MIMO antennas through the incorporation of metamaterial structures has emerged as a key area of research. One effective solution involves overlapping the wave-absorbing frequency band of the metamaterial with the operating band of the antenna. Positioning the metamaterial structure between or around the antenna units acts as a shield against the surface electromagnetic wave propagation caused by coupling between antenna units, thereby enhancing the isolation of the MIMO antenna.

There are three methods of metamaterial loading: horizontal [14–20], vertical [21, 22], and stacking [23–25]. Horizontally loaded metamaterials have become very popular in MIMO antennas because they miniaturize antennas. In [15], a dual-port MIMO antenna with a novel spiral metamaterial structure is proposed. The antenna operates at 3.5 GHz and achieves a gain of 7 dB across the bandwidth, while the isolation of the passband can reach 29.8 dB. A modified W-shaped element and an improved SRR metamaterial are created as a decoupling tool for a multi-band MIMO antenna, as explained in [16]. The isolation in the 6 GHz band was improved by 5 dB. In [17], the authors designed a flower-shaped metamaterial structure consisting of four identical open rings. The flower structure was loaded between the two antenna elements, and the antenna isolation was close to 35 dB at the operating frequency (5.5 GHz). An epsilon-near-zero (ENZ) metamaterial structure is proposed to improve the isolation between two-element antennas in [18]. The isolation was below −20 dB of the operating frequency range. An ultra-broadband MIMO microstrip antenna is reported in [19]. The impedance bandwidth of the proposed MIMO ranged from 2.06 GHz to 15.21 GHz, and its isolation was well below −20 dB. All of the structures previously documented have larger dimensions.

Split-ring resonator (SRR), a typical metamaterial structure, possesses the ability to alter magnetic permeability and effectively minimize the antenna's size. In [20], a modified SRR is introduced, whose antenna achieves a significant reduction in coupling at 38 GHz frequencies, from −17 dB to −47 dB,

* Corresponding author: Yanbing Xue (dlxyb@djtu.edu.cn).

through the integration of an array of three identical metamaterial units. It is shown in [26, 27] that loading open or short stubs inside an SRR can improve resonant characteristics. In [28, 29], the transformation of loaded stubs into fragment-type stubs is proposed, demonstrating the enhancement of sensor and antenna performance by utilizing a loaded fragment-type stub. Moreover, the SRR's shape and loading position can also affect other antenna characteristics such as radiation pattern and impedance matching. However, with the complexity of the structure and the coupling between adjacent structures, the traditional SRR design strongly relies on the researcher's experience and time-consuming iterative simulations. In terms of antenna design, it is difficult to design 5G MIMO antennas loaded with fragment-type SRRs that have both smaller size and higher isolation using classical methods.

To solve this problem, genetic algorithms (GAs) are widely used in antenna optimizations based on their ability to optimize in complex multimodal search spaces [30]. GAs are optimization search algorithms based on the theory of biological evolution. They search for optimal solutions by simulating mechanisms such as selection, crossover, and mutation in the natural evolution process. They can effectively avoid getting trapped in local optima. To obtain the optimal loading positions of fragment-type SRRs, GAs can be utilized for optimization [31].

In this paper, a compact MIMO antenna with high isolation is proposed. The primary contribution is the optimization design of the loaded fragment-type SRRs using GA and High Frequency Structure Simulator (HFSS), which enhances the antenna's design efficiency. Six complementary split-ring resonators (CSRRs) are etched onto a rectangular patch antenna to achieve miniaturization of the antenna element. Subsequently, two antenna elements are horizontally arranged to form a two-port MIMO antenna array. To reduce the mutual coupling in the two-port MIMO antenna, modified fragment-type SRRs are loaded between the antenna elements as a 3×1 array. Taking the antenna isolation as the objective function, the structures and the loading positions of the fragment-type SRRs were optimized using the GA algorithm and HFSS. The electromagnetic characteristics and surface current distribution of the fragment-type SRRs, MIMO antenna performance before and after loading of fragment-type SRRs were investigated by using electromagnetic simulation methods. The feasibility of distributed loading techniques was validated. The MIMO antenna was tested for isolation, impedance bandwidth, envelope correlation coefficient (ECC), diversity gain (DG), total active correlation coefficient (TARC), and channel capacity loss (CCL). Simulations and measurements were conducted and compared. The tests confirmed that fragment-type SRRs loading can better suppress the coupling effect between antennas, making it more efficient to design high-isolation MIMO antennas.

2. EXPERIMENTAL

2.1. Antenna Unit Design

A rectangular patch antenna with an operating frequency of 4.9 GHz was designed, as shown in Fig. 1(a). The MIMO antenna is printed on an FR4 substrate with dimensions 27.5 mm$\times$ 47 mm $\times$ 1.6 mm (a thickness of $h = 1.6$ mm, a relative permittivity of $\varepsilon_r = 4.4$, a dielectric loss tangent of $\tan\delta = 0.02$). Quarter-wavelength impedance transformers are used for impedance matching at the antenna ports. The dimensions of the patch antenna are calculated using Equations (1)–(4). The width of the patch antenna is given by:

$$W = \frac{c}{2f}\sqrt{\frac{2}{(\varepsilon_r + 1)}} \tag{1}$$

The effective dielectric constant of the dielectric material is:

$$\varepsilon_e = \frac{\varepsilon_r + 1}{2} + \frac{\varepsilon_r - 1}{2}\left(1 + 12\frac{h}{W}\right)^{-\frac{1}{2}} \tag{2}$$

The electrical length of the patch antenna is:

$$\Delta L = 0.412h\frac{\varepsilon_e + 0.3}{\varepsilon_e - 0.258} \cdot \frac{\frac{W}{h} + 0.264}{\frac{W}{h} + 0.8} \tag{3}$$

The length of the patch antenna is:

$$L = \frac{c}{2f\sqrt{\varepsilon_e}} - 2\Delta L \tag{4}$$

where c is the speed of light in vacuum.

The initial antenna is simulated and optimized using the parameter scanning method, and the parameters of the antenna are specified as follows (unit: mm): $W_1 = 27.5$, $L_1 = 47$, $W_t = 17.22$, $L_t = 12.93$, $W_g = 0.4$, $L_g = 10$, $W_p = 2.915$, $L_p = 17$. The S-parameter simulation results indicate that the S_{11} is less than -10 dB within the 4.8 to 5.0 GHz frequency range. The antenna operates at a frequency of 4.9 GHz, providing an initial structure for subsequent design.

To achieve antenna miniaturization, a CSRR metamaterial structure is utilized. Parametric simulations of the antenna model, loaded with various CSRR configurations, were performed using HFSS. The results demonstrate that the size, number, and spacing of CSRRs significantly influence the antenna's operating frequency. With six CSRRs of identical dimensions loaded, the antenna operates at 4.92 GHz, as depicted in Fig. 1(a). The CSRR parameters are specified as follows (unit: mm): $O_1 = 3.03$, $I_1 = 2.09$, $I_W = 0.2$, $I_g = 0.2$, $X_d = 0.5$, $Y_d = 0.5$.

2.2. Initial MIMO Antenna Design

The layout of the proposed two-port MIMO antenna is depicted in Fig. 1(b). Employing the parameter sweeping method, the spacing between two antenna units was determined to be 19.19 mm (W_d). The MIMO antenna operates at a frequency of 4.92 GHz, and within the range of 4.84–5.0 GHz, the S_{11} is below -10 dB and S_{21} below -14.73 dB, satisfying the 5G requirements. The final structural dimensions are presented in Table 1.

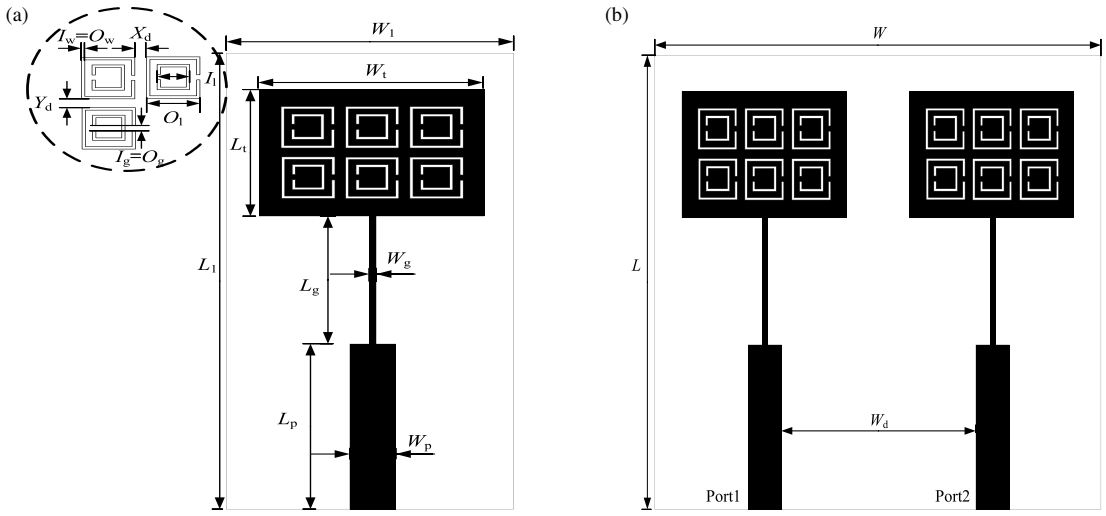

FIGURE 1. Schematic of a MIMO antenna. (a) Antenna element. (b) Front structure.

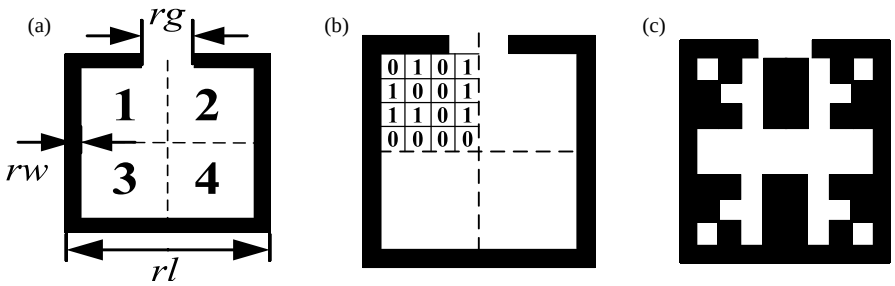

FIGURE 2. Fragment-type SRR. (a) Single SRR ring. (b) Internal grid division. (c) Distributed structure.

TABLE 1. Structure parameters of the MIMO antenna.

Parameter	Value (mm)	Parameter	Value (mm)
W	25	L_p	13.81
L	44	O_1	3.03
W_t	14.63	I_1	2.09
L_t	10.53	I_w	0.2
W_g	0.4	I_g	0.2
L_g	10.83	X_d	0.5
W_p	2.915	Y_d	0.5

2.3. Design Distributed Loading SRRs with GA

To improve the isolation between the antenna units, the fragment-type SRR is shown in Fig. 2. The single SRR structure is shown in Fig. 2(a). The relationship between resonant frequency and LC is:

$$f_0 = \frac{1}{2\pi\sqrt{LC}} \tag{5}$$

where L denotes the equivalent inductance of the total length l of the unopened edge, and C is the equivalent capacitance between two side plates.

$$L = \mu_0 rl \tag{6}$$

$$C = \frac{2\varepsilon_0 rl}{\pi} \ln\left(\frac{2rl}{rg}\right) \tag{7}$$

where μ_0 is the permeability in vacuum, ε_0 the permittivity in vacuum, rl the side length, rw the line width, and rg the opening size.

Assuming that the resonant frequency of the SRR is $f_0 = 4.9$ GHz, its initial dimensions can be calculated using Equations (5)–(7): $rl = 6$ mm, $rw = 0.3$ mm, $rg = 3.5$ mm.

In the manufacturing process of fragment-type SRRs, it is not possible to use empirical formulas to design the distribution of metal units due to the inherent randomness of the process. The structural parameters and loading position of the fragment-type SRRs must be continuously adjusted to satisfy the design requirements of the antenna. To improve the design efficiency, a co-simulation approach using HFSS and MATLAB software is used. The optimization flowchart is shown in Fig. 3. The parameters of the fragment-type SRRs and loading position are considered optimization variables, and the optimization of the antenna is performed using the GA algorithm.

The unique aspect of the optimization method proposed in this work is our subgrids coding method. The method is divided into three main steps:

1) The single SRR was divided into four basic subgrid structures, which is shown in Fig. 2(a).

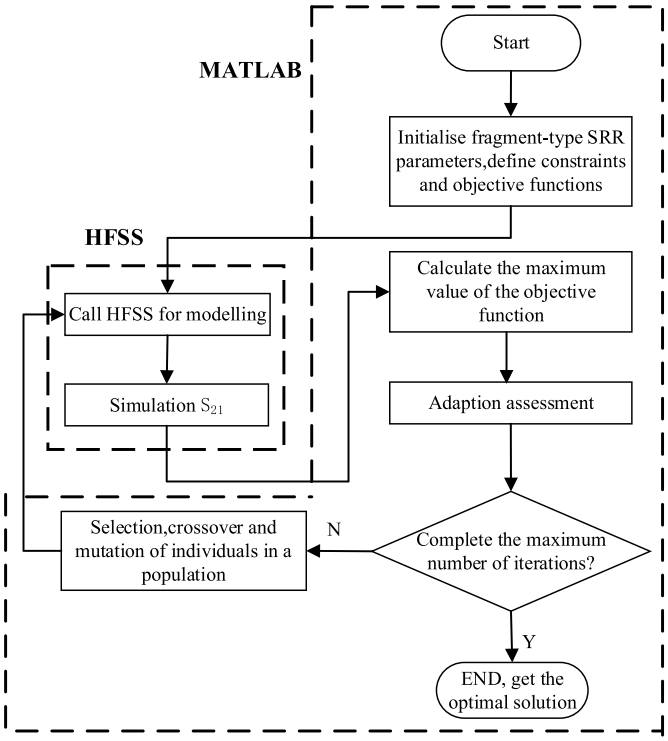

FIGURE 3. Flowchart of the GA and HFSS co-simulation optimization.

2) Subgrid 1 was divided into 4×4 small cells, each 0.6 mm $\times$ 0.6 mm, and subgrids 2, 3, and 4 were derived from subgrid 1. The structures are shown in Fig. 2(b). Each cell represents a dimension to be optimized, where the binary "1" represents a metal conductor, and the binary "0" represents no conductor.

3) The global search GA algorithm was used to optimize the 0-1 matrix obtained to construct the fragment-type SRRs. In addition, *rl*, *rw*, and *rg* are three consecutive parameters to be optimized.

The objective function fitness of the GA algorithm was set as the S_{21} of the antenna at 4.9 GHz. Fitness was calculated as shown in Equation (8). In order to improve the isolation of the MIMO antenna, a smaller fitness value is better.

$$\text{Fitness} = S_{21}(f_{4.9\,\text{GHz}}) \tag{8}$$

The initial population size was set to 200, and the maximum number of iterations was 15. The optimization variables were the structural parameters of the single SRR ($0 < rl < 6$ mm, $0 < rw < 0.3$ mm, $0 < rg < 3.5$ mm). An Intel Corei5-7200 CPU was used for the computation, and the optimized SRRs' dimensions were obtained after 3000 simulations, which took about 440 hours. The approximate Pareto solution set was obtained, yielding the following optimization parameters (unit: mm): $rl = 5.418$, $rw = 0.229$, $rg = 2.947$. The 0-1 matrix inside SRR $= [0\,1\,0\,1; 1\,0\,0\,1; 1\,1\,0\,1; 0\,0\,0\,0]$. Therefore, we can generate a lot of subgrids to optimize the effective size of the metal patch by fragment-type SRR structure in Fig. 2(c).

2.4. Optimizing the MIMO Antenna with the Fragment-Type SRRs

After co-simulation using GA and HFSS, the structure of the MIMO antenna loaded with fragment-type SRRs proposed in this paper is shown in Fig. 4. The simulation demonstrates that the opening positions and spacing (*rd*) of the fragment-type SRRs significantly affect the reflection efficiency of the MIMO antenna unit, especially when the SRRs are loaded with the same edge length but different opening positions and orientations. When a Y-axis symmetric configuration was selected for the SRRs, with a distance *rd* of 2.874 mm, the reflection coefficients S_{11} and S_{22} were practically identical. This symmetry ensures that the reflection coefficient of the MIMO antenna unit remains unaffected.

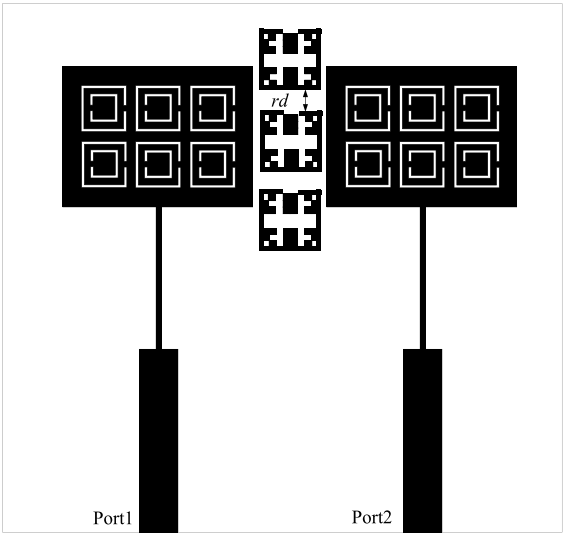

FIGURE 4. Front structure of MIMO antenna after loading metamaterials.

2.5. Fabrication and Measurement of MIMO Antenna

Experimental validation of the proposed two-port MIMO antenna incorporating the fragment-type SRRs was conducted. The antenna was fabricated using an FR4 substrate, and S-parameter measurements were performed using a Ceyear 3656B vector network analyzer. The fabricated antenna and corresponding measurement setup are depicted in Fig. 5. The frequency sweep for this test was configured to range from 4 GHz to 6 GHz with an excitation power of 10 dBm. The Calibration Kits for 3656B using TOSM calibration standards were adopted.

3. SIMULATION

3.1. S-Parameters

Figure 6 presents a comparative analysis of the simulated antenna's S-parameters under four conditions: as an antenna element, unloaded (no SRR), loaded with only SRRs, and loaded with fragment-type SRRs. Fig. 6(a) shows the reflection coefficient curves of the MIMO antenna, highlighting the vari-

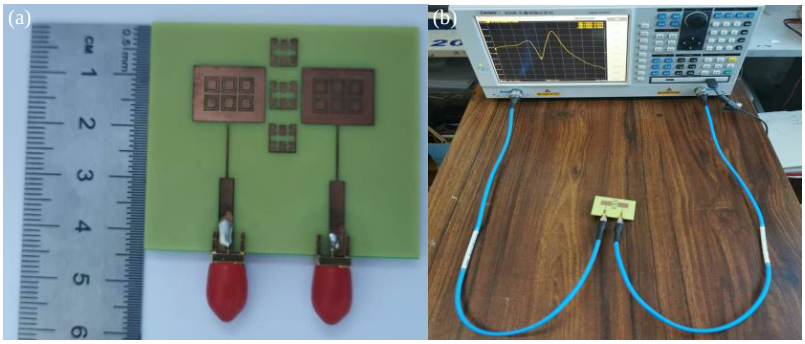

FIGURE 5. Fabricated antenna. (a) Front view and scale. (b) Test setup.

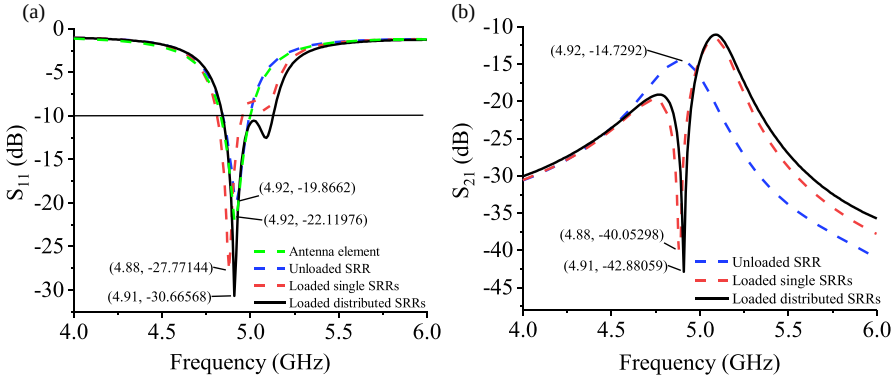

FIGURE 6. Comparison of the S-parameters of a MIMO antenna before and after loading distributed SRRs. (a) Reflection coefficient. (b) Transmission coefficient.

ations in the performance of the fragment-type SRRs before and after their implementation. At 4.92 GHz, the S_{11} of the MIMO antenna element and unloaded SRR were -22.11 dB and -19.87 dB, respectively. After loading only SRRs and fragment-type SRRs, the S_{11} of the MIMO antenna decreased to -27.77 dB and -30.66 dB, respectively. The SRRs resonate at the antenna's operating frequency, thereby enhancing its reflection coefficient.

In terms of the -10 dB bandwidth, the impedance bandwidth of the individual antenna element is 0.15 GHz (4.84–4.99 GHz). For the antenna unloaded SRRs, the impedance bandwidth is 0.14 GHz (4.84–4.99 GHz). When only SRRs are loaded, the impedance bandwidth of the antenna is 0.13 GHz (4.82–4.95 GHz). The antenna loaded with fragment-type SRRs exhibits the largest impedance bandwidth, which is 0.19 GHz (4.85–5.04 GHz).

Furthermore, Fig. 6(b) shows the transmission coefficient curves, which illustrate the isolation levels for three conditions. The results reveal that the mutual coupling among all antennas with unloaded SRRs was -14.73 dB. In the frequency band of 4.84 to 5 GHz, the S_{21} for configurations loaded with only SRRs and fragment-type SRRs exhibited a minimum isolation of -40.05 dB and -42.88 dB, respectively. It is evident that loading with fragment-type SRRs contributes to the enhanced performance of the MIMO antenna system.

3.2. Radiation Patterns

Figure 7 shows the radiation patterns of the MIMO antenna in the E-plane and H-plane at 4.9 GHz under three conditions: unloaded (no SRR), loaded with only SRRs, and loaded with fragment-type SRRs. The figure also shows the co-polarized and cross-polarized patterns of each plane. The results demonstrate that the incorporation of fragment-type SRRs has a certain influence on the main polarization and cross-polarization radiation patterns of the E-plane and H-plane for a dual-element microstrip array antenna arranged in the H-plane. However, the variations are minimal and within an acceptable range, with the cross-polarization levels being more than 30 dB below the co-polarization levels. It is due to the placement of the fragment-type SRRs between the antenna units, which avoids interference with the radiation pattern.

3.3. Radiation Efficiency

Figure 8 illustrates the radiation efficiency of the MIMO antenna with fragment-type SRRs. The simulated radiation efficiency is consistently above 55% (4–5.54 GHz), and reaches a peak of 67% at the 4.81 GHz. This meets the typical requirements for MIMO antenna radiation efficiency.

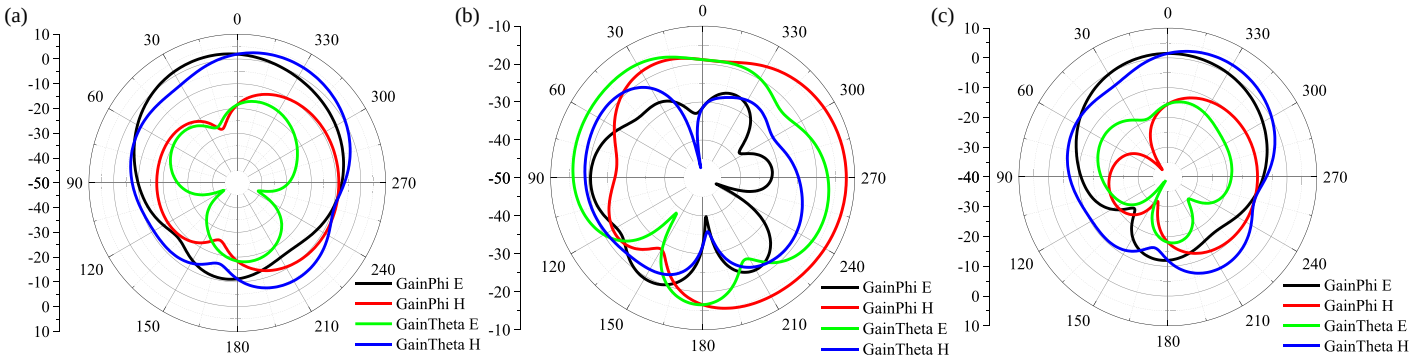

FIGURE 7. Radiation patterns of the MIMO antenna at 4.9 GHz. (a) Unloaded SRR. (b) Loaded only SRRs. (c) Loaded fragment-type SRRs.

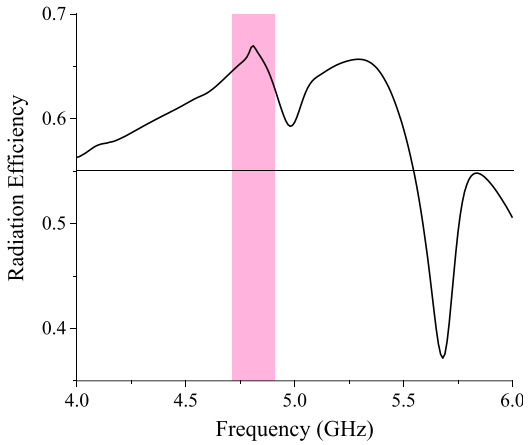

FIGURE 8. Radiation efficiency of the MIMO antenna.

3.4. Mechanism of Distributed Loading

In order to verify the metamaterial properties of the proposed fragment-type SRRs, the equivalent permittivity and equivalent permeability are extracted to analyze the structural properties. The relevant equations are:

$$\mu_r = nz \tag{9}$$

$$\varepsilon_r = n/z \tag{10}$$

where z denotes the equivalent impedance, and n signifies the equivalent refractive index. Both can be obtained using the following equations:

$$z = \sqrt{\frac{(1+S_{11})^2 - S_{21}^2}{(1-S_{11})^2 - S_{21}^2}} \tag{11}$$

$$n = \frac{1}{kh}\cos^{-1}\left[\frac{1}{2S_{21}}\left(1 - S_{11}^2 + S_{21}^2\right)\right] \tag{12}$$

where S_{11} is the return loss, S_{21} the insertion loss, k the free space incident wave number, and h the thickness of the dielectric substrate.

The equivalent permittivity and equivalent permeability were calculated by the S-parameters inversion method, as shown in Fig. 9.

The single SRR has a positive real part of its equivalent permittivity and a negative real part of its equivalent permeability (in the range of 4.76 to 4.87 GHz). Furthermore, the fragment-type SRR has a positive real part of its equivalent permittivity and a negative real part of its equivalent permeability in the 5.09 to 5.18 GHz range. It can be seen that both structures are single-negative permeability metamaterials. In addition, single-negative permeability metamaterials cause sharp attenuation of specific frequency electromagnetic waves in the structure, which can effectively suppress electromagnetic coupling between antenna units.

The fragment-type SRRs can be equivalent to many capacitors and inductors connected in parallel, which improves its resonant frequency. The real part of its equivalent permeability decreases; the electrical conductivity decreases; and the electromagnetic wave attenuation increases. Overall, it can be seen that loading fragment-type SRRs can effectively improve the electromagnetic properties of metamaterials.

3.5. Surface Current Distribution

The surface current distributions of the SRR and MIMO antenna are shown in Fig. 10. In Fig. 10(a), the current is mainly distributed in the loop portion of the single SRR. In Fig. 10(b), the current is distributed in the loading region of the metal unit inside the SRR, where the current distribution is relatively concentrated. The comparison reveals that the maximum surface current after loading the fragment-type SRR is 2.4 times higher than that before loading. Evidently, the use of the fragment-type SRRs can enhance the intensity of the surface current within the SRR. The resonance frequency is mainly determined by the maximum internal current loop after loading, which can be adjusted by changing the current loop path length by optimizing the position of the fragments.

In Fig. 10(c), both antenna units without loaded fragment-type SRRs have a current distribution, and the surface current of the left antenna unit is more densely distributed than the right one. In Fig. 10(d), with the loaded fragment-type SRRs as center symmetry, its left antenna unit features a dense current distribution, and the surface of the right antenna unit shows almost no current distribution. The results demonstrate that the loaded fragment-type SRRs can reduce the coupling between the two antenna units and improve the isolation of the MIMO antenna.

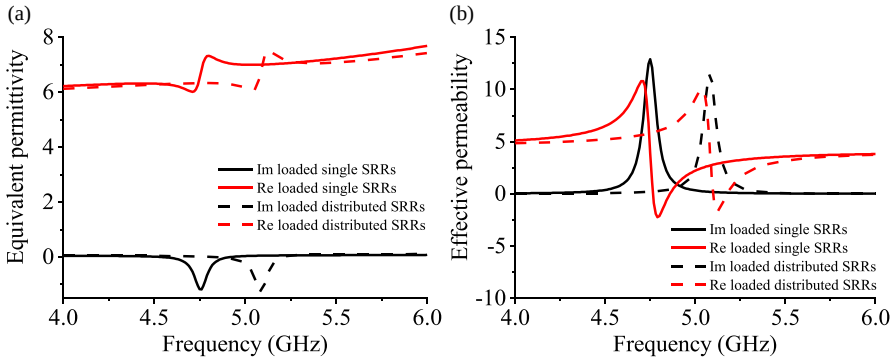

FIGURE 9. Equivalent permittivity and permeability of SRR ring. (a) Equivalent permittivity. (b) Equivalent permeability.

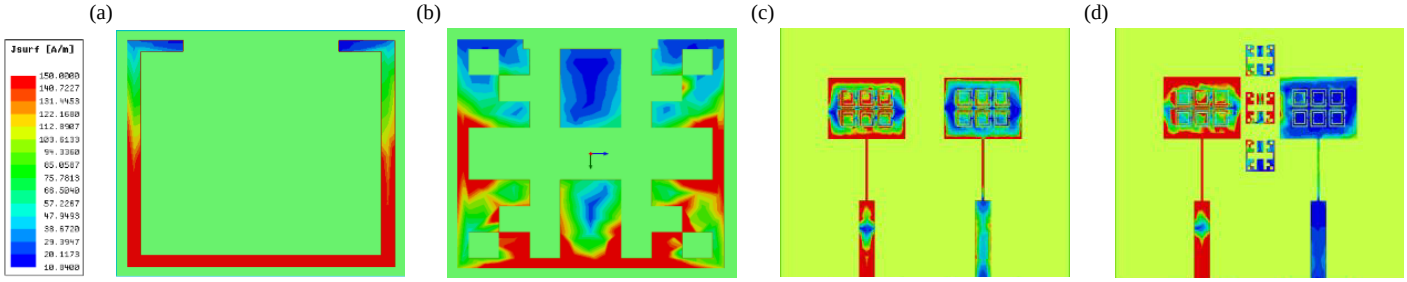

FIGURE 10. Obtained surface current distribution. (a) Single SRR. (b) Fragment-type SRR. (c) MIMO antenna unloaded SRR. (d) MIMO antenna loaded with fragment-type SRRs.

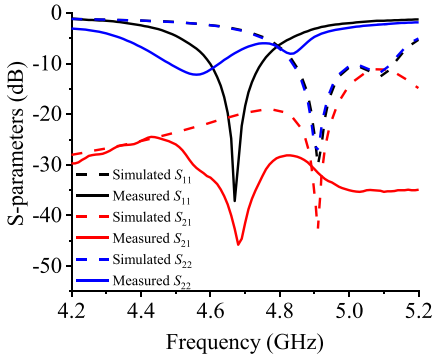

FIGURE 11. Measured and simulated S-parameters.

4. RESULTS AND DISCUSSION

4.1. Test Results of the MIMO Antenna S-Parameters

Figure 11 illustrates the comparison between the measured and simulated S-parameters of the antenna system. As depicted in the figure, the measured and simulated -10 dB impedance bandwidths are 3.2% (4.6–4.75 GHz) and 3.25% (4.85–5.04 GHz), respectively. Specifically, at 4.67 GHz, the S_{11} parameter is better than -37 dB, and the S_{21} parameter is below -42 dB, indicating that the MIMO antenna achieved high isolation.

In the simulation, the S_{11} and S_{22} parameters are nearly coincident, with only minor variations observed at the operating frequency of 4.91 GHz. However, during the measurements, a significant discrepancy was observed between S_{11} and S_{22}, deviating from the simulated outcomes. This divergence is likely attributed to the impact of the connectors, as port 1 was not properly terminated with a 50 ohm load during the S-parameter measurement at port 2.

4.2. Diversity Characteristic Analysis

In a MIMO system, determining the effective bandwidth only based on the scattering matrix is insufficient; thus, the envelope correlation coefficient (ECC), diversity gain (DG), total active correlation coefficient (TARC), and channel capacity loss (CCL) must also be considered [26].

Comparisons of the simulated and measured values for ECC, DG, TARC, and CCL are shown in Fig. 12. The analysis depicted in Fig. 12(a) reveals that the ECC values of the proposed MIMO antenna are less than 0.05, indicating that they are close to 0 at all operating frequencies. This value is considered significantly low, as obtained through evaluating ECC from far-field radiation patterns. Additionally, based on the ECC, the proposed MIMO antenna achieves a DG of 9.98 dB, indicating an excellent performance in diversity analysis.

Furthermore, based on the simulated and measured results, the TARC and CCL values are determined. A TARC value of less than -10 dB indicates minimal reflection, meaning that the antenna is radiating power efficiently. A CCL value below 0.4 bits/sec/Hz is considered for an enhanced MIMO antenna performance. As shown in Fig. 12(b), the TARC values are recorded at -20 dB for the 4.67 GHz band and -30 dB for the 4.9 GHz band. The CCL values average 0.2 bits/sec/Hz for the 4.67 GHz band and 0.03 bits/sec/Hz for the 4.9 GHz band. The simulated and measured results exhibit only minor discrepancies, which fall within an acceptable range, thereby confirming the reliability of the antenna design.

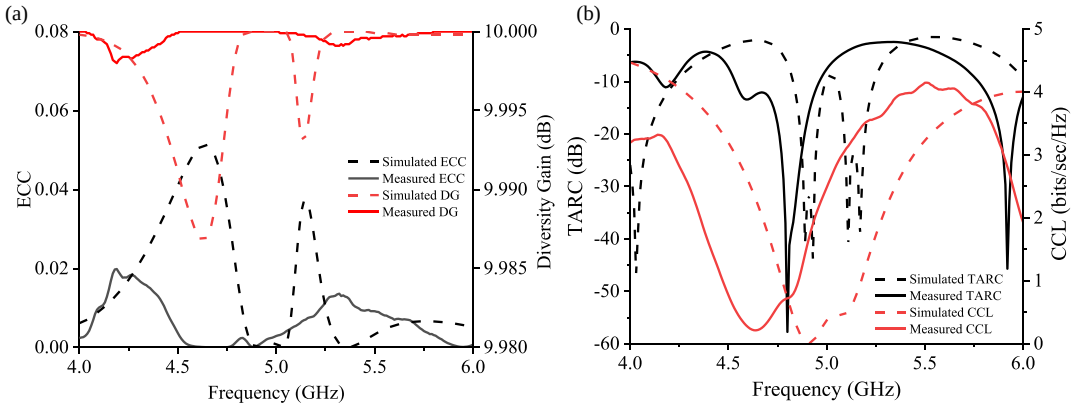

FIGURE 12. Diversity analysis. (a) ECC and diversity gain. (b) TARC and CCL.

TABLE 2. Performance comparison with other MIMO antennas.

Ref.	Operating frequency (GHz)	−10 dB Bandwidth (GHz)	Isolation (dB)	Board Size (mm^2)	ECC
[14]	3.5	3.5–3.55	28	76.4×91	–
[15]	3.5	3.42–3.52	22	55×50	0.02
[16]	3.94	3.45–4.1	16	70×40	< 0.005
[17]	5.5	–	34.77	–	0.00043
[18]	3.7	3–6	40.58	66×36	0.025
[19]	13.2	2–15	> 20	89×30	0.0014
[20]	28 38	27.1–28.8 35.2–38.9	34.6/47	26×14	< 0.02
This work	4.9	4.84–5	42.88	55×44	0.0042

A deviation in the 4.9 GHz frequency band is observed when comparing the simulated and measured results, which can be attributed to several factors: (1) The simulation assumes an ideal dielectric constant of 4.4 for the FR4 substrate. However, the actual dielectric constant of the antenna's plate may vary, introducing discrepancies. (2) Processing errors, such as those introduced during printed circuit board (PCB) printing and SMA head welding, can affect the antenna's performance. (3) Because the test is conducted in a conventional electromagnetic environment, a low-magnitude response is very sensitive to the environment and fabrication tolerance.

4.3. Comparison with Other Research

Table 2 compares the antenna performance with reference to other literature. All metamaterial structures are horizontally integrated into these MIMO antennas. It is evident that most of the referenced works [14–16, 18, 19] have large dimensions, except [17, 20]. In contrast, the proposed MIMO antenna achieves a relatively compact structure by etching six CSRRs. Furthermore, this work provides a remarkable improvement in isolation at lower frequencies compared to the previous works [14–17]. Although some literature reports excellent ECC values, such as those in [17, 19], the proposed antenna exhibits an almost exceptional performance in terms of ECC. It is obvious that our MIMO antenna is better with regard to the size, isolation, and ECC.

5. CONCLUSIONS

This paper has introduced a 5G high-isolation MIMO antenna with fragment-type SRRs. Miniaturization of the 4.9 GHz antenna unit was achieved by etching 6 CSRRs onto the antenna radiating patch. The fragment-type SRRs were loaded horizontally between two antenna units as 3×1 arrays, and the structure and loading position of the fragment-type SRRs were optimized using a GA and HFSS co-simulation. In this way, the high isolation of antenna units could be achieved in the MIMO antenna array. The MIMO antenna array described in this paper has dimensions $50\,\text{mm} \times 44\,\text{mm} \times 1.6\,\text{mm}$, which resulted in an impedance bandwidth of 0.19 GHz. The isolation at the antenna operating frequency was 42.88 dB, which is 28.15 dB higher than the isolation without the unloaded distributed SRRs. Diversity characteristics were also examined, and better results were achieved in terms of ECC (ECC < 0.0042), DG, TARC, and CCL. The proposed MIMO antenna has been simulated and measured successfully, and the test verified that the fragment-type SRRs can effectively suppress the coupling of antenna units and provide a new method to improve the isolation of MIMO antennas.

ACKNOWLEDGEMENT

This work was supported by the Applied Basic Research Project of Liaoning Science and Technology Department under Grant ID 2022JH2/101300267.

REFERENCES

[1] Bilal, M., S. I. Naqvi, N. Hussain, Y. Amin, and N. Kim, "High-isolation MIMO antenna for 5G millimeter-wave communication systems," *Electronics*, Vol. 11, No. 6, 962, 2022.

[2] Lin, B. J., X. W. Chen, and J. R. Su, "Compact and high isolation dual-band MIMO antenna for 5G wireless communication," *J. of Test and Measurement Tech.*, Vol. 37, No. 1, 87–92, Feb. 2023.

[3] Sharawi, M. S., "Printed multi-band MIMO antenna systems and their performance metrics [Wireless corner]," *IEEE Antennas and Propagation Magazine*, Vol. 55, No. 5, 218–232, 2013.

[4] Hu, W., Q. Li, H. Wu, Z. Chen, L. Wen, W. Jiang, and S. Gao, "Dual-band antenna pair with high isolation using multiple orthogonal modes for 5G smartphones," *IEEE Transactions on Antennas and Propagation*, Vol. 71, No. 2, 1949–1954, 2023.

[5] Tiwari, R. N., P. Singh, S. Pandey, R. Anand, D. K. Singh, and B. K. Kanaujia, "Swastika shaped slot embedded two port dual frequency band MIMO antenna for wireless applications," *Analog Integrated Circuits and Signal Processing*, Vol. 109, No. 1, 103–113, 2021.

[6] Trivedi, K. and D. Pujara, "Mutual coupling reduction using defected ground structure in UWB DRA array for MIMO application," in *2020 IEEE International Symposium on Antennas and Propagation and North American Radio Science Meeting*, 1879–1880, Montreal, QC, Canada, 2020.

[7] Harbel, M., J. Zbitou, M. Hefnawi, and M. Latrach, "Mutual coupling reduction in mmWave patch antenna arrays using mushroom-like EBG structure," in *2020 IEEE 2nd International Conference on Electronics, Control, Optimization and Computer Science (ICECOCS)*, 1–3, Kenitra, Morocco, 2020.

[8] Alibakhshikenari, M., F. Babaeian, B. S. Virdee, S. Aïssa, L. Azpilicueta, C. H. See, A. A. Althuwayb, I. Huynen, R. A. Abd-Alhameed, F. Falcone, and E. Limiti, "A comprehensive survey on "Various decoupling mechanisms with focus on metamaterial and metasurface principles applicable to SAR and MIMO antenna systems"," *IEEE Access*, Vol. 8, 192 965–193 004, 2020.

[9] Das, S., D. Mitra, and S. R. B. Chaudhuri, "Fractal loaded planar super wide band four element MIMO antenna for THz applications," *Nano Communication Networks*, Vol. 30, 100374, 2021.

[10] Rajkumar, S., A. A. Amala, and K. T. Selvan, "Isolation improvement of UWB MIMO antenna utilising molecule fractal structure," *Electronics Letters*, Vol. 55, No. 10, 576–579, 2019.

[11] Raheja, D. K., B. K. Kanaujia, and S. Kumar, "Compact four-port MIMO antenna on slotted-edge substrate with dual-band rejection characteristics," *International Journal of RF and Microwave Computer-Aided Engineering*, Vol. 29, No. 7, e21756, 2019.

[12] Khan, A., Y. He, Z. He, and Z. N. Chen, "A compact quadruple-band circular polarized MIMO antenna with low mutual coupling," *IEEE Transactions on Circuits and Systems II: Express Briefs*, Vol. 70, No. 2, 501–505, 2023.

[13] Tang, M. C., Z. Y. Chen, Z. L. Shi, and R. W. Ziolkowski, "Mutual coupling reduction using meta-structures for wideband, dual-polatized, and high-density arrays," *IEEE Transactions on Antennas and Propagation*, Vol. 65, No. 8, 3986–3998, 2017.

[14] Yang, X. M., X. G. Liu, X. Y. Zhou, and T. J. Cui, "Reduction of mutual coupling between closely packed patch antennas using waveguided metamaterials," *IEEE Antennas and Wireless Propagation Letters*, Vol. 11, 389–391, 2012.

[15] Feng, X. X., Y. L. Luo, and C. C. Qi, "Design of a high-isolation MIMO antenna based on a new metamaterial structure," in *2018 National Conference on Microwave and Millimeter Wave*, 1336–1440, CNKI, 2018.

[16] Sharma, R., R. Khanna, and Geetanjali, "Compact sub-6 GHz and mmWave 5G wideband 2×1 MIMO antenna with high isolation using parasitically placed double negative (DNG) isolator," *Wireless Personal Communications*, Vol. 122, No. 3, 2839–2857, 2022.

[17] Garg, P. and P. Jain, "Isolation improvement of MIMO antenna using a novel flower shaped metamaterial absorber at 5.5 GHz WiMAX band," *IEEE Transactions on Circuits and Systems II: Express Briefs*, Vol. 67, No. 4, 675–679, 2020.

[18] Supreeyatitikul, N., A. Phungasem, and P. Aeimopas, "Design of wideband sub-6 GHz 5G MIMO antenna with isolation enhancement using an MTM-inspired resonators," in *2021 Joint International Conference on Digital Arts, Media and Technology with ECTI Northern Section Conference on Electrical, Electronics, Computer and Telecommunication Engineering*, 206–209, Chaam, Thailand, 2021.

[19] Shelar, O. A., T. Ali, and P. Kumar, "UWB-MIMO antenna for wireless communication systems with isolation enhancement using metamaterial," in *2022 16th European Conference on Antennas and Propagation (EuCAP)*, 1–5, Madrid, Spain, 2022.

[20] Esmail, B. A. F. and S. Koziel, "Design and optimization of metamaterial-based dual-band 28/38 GHz 5G MIMO antenna with modified ground for isolation and bandwidth improvement," *IEEE Antennas and Wireless Propagation Letters*, Vol. 22, No. 5, 1069–1073, 2023.

[21] Madni, A., R. M. H. Bilal, and W. T. Khan, "A compact metamaterial based high isolation MIMO antenna for 5.8 GHz WLAN applications," in *2022 IEEE International Symposium on Antennas and Propagation and USNC-URSI Radio Science Meeting (AP-S/URSI)*, 245–246, Denver, CO, USA, 2022.

[22] Nie, Z. H., "Metamaterial-based 5G base station antenna research," M.S. thesis, Xidian University, Xian, China, 2020.

[23] Zhang, S., "Metamaterial-based multifrequency antenna and high isolation MIMO antenna, China," M.S. thesis, Nanjing University of Posts and Telecommunications, Nanjing, China, 2020.

[24] Dey, S., S. Dey, and S. K. Koul, "Isolation improvement of MIMO antenna using novel EBG and hair-pin shaped DGS at 5G millimeter wave band," *IEEE Access*, Vol. 9, 162 820–162 834, 2021.

[25] Jiang, J., Y. Li, L. Zhao, and X. Liu, "Wideband MIMO directional antenna array with a simple meta-material decoupling structure for X-band applications," *Applied Computational Electromagnetics Society Journal*, Vol. 35, No. 5, 556–566, 2020.

[26] Khan, A., Y. He, and Z. N. Chen, "An eight-port circularly polarized wideband MIMO antenna based on a metamaterial-inspired element for 5G mmWave applications," *IEEE Anten. and Wirel. Propag. Lett.*, Vol. 22, No. 7, 1572–1576, 2023.

[27] Athukorala, L. and D. Budimir, "Design of compact dual-mode microstrip filters," *IEEE Transactions on Microwave Theory and Techniques*, Vol. 58, No. 11, 2888–2895, 2010.

[28] Ding, D. W., "MOEA/D-based optimization techniques and their application in antenna design," Ph.D. dissertation, University Science and Technology of China, Hefei, China, 2015.

[29] Ting, L., "Miniaturization and application of microstrip open-loop resonator loaded with fragments," M.S. thesis, University Science and Technology of China, Hefei, China, 2017.

[30] Weile, D. S. and E. Michielssen, "Genetic algorithm optimization applied to electromagnetics: A review," *IEEE Transactions on Antennas and Propagation*, Vol. 45, No. 3, 343–353, 1997.

[31] Wang, S., Y. B. Xue, Z. Song, B. J. Chen, and C. Feng, "Inkjet-printed chipless RFID humidity sensor based on paper substrate," *Chinese J. of Scientific Instr.*, Vol. 41, No. 3, 150–158, 2020.